Suppressed Blinking and Auger Recombination in Near-Infrared Type-II InP/CdS Nanocrystal Quantum Dots

Allison M. Dennis, Benjamin D. Mangum, Andrei Piryatinski, Young-Shin Park, Daniel C. Hannah, Joanna L. Casson, Darrick J. Williams, Richard D. Schaller, Han Htoon, and Jennifer A. Hollingsworth

Supporting Information

Materials and Synthetic Methods.

Materials. Indium (III) acetate (99.99%-In, puratrem) was procured from Strem Chemicals (Newburyport, MA). Myristic acid (99.5+%), octadecene (ODE; 90%, technical grade), and oleylamine (approx. C18 content 80-90%) were purchased from Acros Organics (Morris Plains, NJ). Oleic acid (technical grade, 90%) and cadmium oxide (CdO, 99.95+%, metals basis) were bought from Alfa Aesar (Ward Hill, MA). All chemicals were used as purchased, except hexane and ethanol from Fisher Chemicals (Fair Lawn, NJ), which were sparged with Ar prior to exposure to InP cores.

Methods. NQD Synthesis. *Precursors*. A 0.08 M stock solution of indium myristate (In:MA 1:4) was prepared by mixing 4 mmol indium (III) acetate (1.168 g) and 16 mmol myristic acid (3.654 g) in 50 mL ODE at 120°C under vacuum for several hours. A 0.13 M stock solution of tris(trimethylsilyl)phosphine [$(TMS)_3P$] in oleylamine and ODE was prepared by mixing 487 μL $(TMS)_3P$ (1.6 mmol), 9.04 mL oleylamine (19.2 mmol), and 2.5 mL ODE in a glovebox. A 1 M stock solution of cadmium oleate in oleic acid (1 M $Cd(OA)_2$, 1:2.8 Cd:OA) was prepared by mixing 0.1 mol CdO (12.84 g) and 100 mL oleic acid (0.28 mol, 89.1 g) in a 250 mL round-

bottom flask. The rust-colored mixture was degassed at 100°C under vacuum, prior to the temperature being raised to 280°C under argon flow. After the solution clarified, the temperature was reduced to 100°C and vacuum was applied to remove water that was generated during the formation of cadmium oleate. A 0.2 M solution of $Cd(OA)_2$ with a 1:4 Cd:OA was prepared by diluting 20 mL of the 1 M $Cd(OA)_2$ stock with 8.45 mL oleic acid and 71.5 mL ODE. A 0.2 M solution of sulfur in ODE was prepared by dissolving 0.2 mol sulfur in 100 mL ODE at 80°C under vacuum.

InP core synthesis. The InP core synthesis was adapted from a previously reported procedure.[1] In a 100 mL round-bottom flask with condenser, 5 mL of the indium myristate stock solution was heated to 188°C. Several syringes containing $(TMS)_3P$ stock solution were removed from the glovebox and added to the indium myristate solution as follows: a 1.5 mL bolus of $(TMS)_3P$ was injected and the temperature dropped to 178°C, where it was maintained. After 45 s, another 1.5 mL of $(TMS)_3P$ was added to the solution dropwise over the span of 1 min. After another minute of growth, 5 mL of the indium myristate stock solution was added to the reaction solution and the solution temperature was allowed to stabilize at 178°C (~3 min). Three mL of $(TMS)_3P$ were added dropwise over 3 min. The addition of 5 mL In:MA and 3 mL $(TMS)_3P$ was repeated once more, followed by a rapid reduction in temperature upon the injection of 20 mL of degassed ODE. Cores were stored as a waxy solid in the reaction solution at 4°C, protected from air and light.

InP/CdS core/shell synthesis. In Ar-filled septa-capped tubes, InP cores were diluted with hexane and ethanol prior to centrifugation at 5000 rpm. The majority of the NQDs formed an oily film on the tube, which was readily resuspended in hexane. The core size and concentration was calculated from the 1S peak in the absorption spectrum, as described in the literature.[2] In a 250

mL round-bottom flask with condenser, 5 mL of oleylamine and 3 mL of ODE were degassed. Washed cores in hexane (3.7 mL, 44 μM) were added and the solvent subsequently removed under vacuum with the temperature gradually raised to 100°C. The reaction flask was backfilled with Ar and the temperature was further raised to 150°C. The first cation addition, 0.73 mL 0.2 M $Cd(OA)_2$, was added dropwise and the mixture allowed to react for 10 min, followed by dropwise addition of 0.73 mL 0.2 M sulfur in ODE. (Note: the first addition of cadmium oleate and the initial annealing step were conducted at 150°C due to an observed sensitivity of the InP core to etching at high temperatures under these reaction conditions, *i.e.*, in presence of oleylamine and/or with these particular shell precursors). The temperature was immediately raised to 240°C for all subsequent precursor additions and anneals. The first shell was annealed for 30 min at this elevated temperature. All subsequent shells were annealed at 240°C for ~2.5 h following the injection of the cation ($Cd(OA)_2$) and ~1 h following dropwise addition of the anion (sulfur in ODE). Cation/anion addition volumes for shell addition cycles 2-10 were as follows: 0.83, 1.04, 1.26, 1.31, 1.54, 1.80, 1.79, 2.04, and 2.31 mL, respectively. Large samples of the reaction solution were taken after 1, 4, 7, and 10 shells (1, 2, 3, and 4 mL, respectively) and stored "raw", *i.e.,* in the reaction solution, at 4°C for future analysis; precursor addition volumes took the removal of these large samples into account. Very small volumes of the reaction solution (a couple of drops) were collected after the intermediate shells were added (*i.e.,* 2, 3, 5, 6, 8, and 9) and stored in hexane following precipitation with ethanol. The raw samples could be worked up and analyzed "fresh" months after the reaction, while the worked up samples have less stability than the raw solutions due to the dilution of the NQDs.

A JEOL 2010 operating at 200 kV was used to perform the transmission electron microscopy (TEM) studies. The size of the resulting NQDs was determined by manually circling hundreds of

dots in TEM images in Igor Pro software.

Spectroscopy. Absorption spectra were collected on a Cary Varian 5000 UV-Vis-NIR spectrophotometer after NQDs were precipitated with ethanol and resuspended in hexane. PL spectra were collected on a Horiba Yobin Jvon NanoLog spectrofluorimeter using a 450 W Xe arc lamp for excitation and a photomultiplier tube (PMT) for visible detection (to 850 nm) and a LN-cooled InGaS CCD array for detection above 800 nm. Spectra were corrected for grating and detector inefficiencies and to minimize hexane reabsorption effects in the NIR. NQDs diluted in hexane were excited at 405 nm with a slit width of 5 nm. Emission from 450 – 800 nm was measured with 0.1 s integration time and a 5 nm emission slit width. Emission >800 nm was measured with 1 s integration and 20 nm emission slit width. The spectral intensities were plotted across the entire wavelength range by multiplying the NIR emission spectra by a standard scaling factor determined by examining the overlap of the two spectra from 800 to 850 nm. The transition from one detector to another is indicated in Figure 2a by the dotted grey line at 800 nm. The shoulders seen in the PL spectra around this region are assumed to be artifacts of splicing together spectra from two different detectors and/or related to using the detectors at the edges of their operational windows. PLE spectra were collected using Xe lamp excitation with 0.05 s integration.

Ensemble lifetime measurements were performed by drop-casting films of NQDs on glass substrates and illuminating under pulsed wide-field excitation (405 nm, 70 ps pulsewidth) at a repetition rate of either 125 kHz or 250 kHz. The resulting PL was collected with a 100x 1.3 NA objective and passed through an appropriate long-pass filter and finally directed onto a single-photon avalanche photodiode (APD, Perkin Elmer SPCM AQR-14). Time correlated single photon counting (TCSPC) electronics were used to timestamp the arrival time of each photon.

Lifetimes were determined by fitting the histograms of time delays between laser excitation and PL emission. The fits were tri-exponential fits of the form:

$$y = y_0 + A_1\, exp\left(-\frac{(x-x_0)^2}{\tau_1}\right) + A_2\, exp\left(-\frac{(x-x_0)^2}{\tau_2}\right) + A_3\, exp\left(-\frac{(x-x_0)^2}{\tau_3}\right)$$

Average lifetime values reported are calculated using the various fit components as follows:[3]

$$\tau_{avg} = \sum_n \frac{A_n \tau_n^2}{\sum_m A_m \tau_m}$$

The resulting PL lifetime fit parameters are listed in Table S1.

Time-resolved PL (tr-PL) measurements were also performed by photo-exciting stirred dispersions of NQDs in hexane at controlled intensity using 35 fs pulses at 400 nm and 2 kHz repetition rate. Tr-PL signals were collected and directed to a 150 mm focal length spectrograph and photo-counting streak camera. Streak camera data was spectrally integrated in order to produce tr-PL temporal decay profiles. Following normalization of tr-PL decay profiles at long delay times, low pump-intensity data was subtracted from profiles collected at higher-pump-intensity so as to reveal multi-exciton decay dynamics, which were then fitted using a single exponential decay.

For blinking measurements, InP/CdS NQDs were first greatly diluted in hexane and drop-cast on a quartz substrate. NQD density was estimated to be ~0.05-0.1 NQD/μm^2, ensuring measurement of single NQDs. A continuous wave (CW) laser at 405 nm was used to excite individual NQDs through a 100x, 0.8 NA (numerical aperture) objective lens that was also used for collecting PL emission from single NQDs. The photons in PL emission were recorded using an avalanche photodiode (APD) in time-tagged single photon counting mode and PL intensity time-trace was analyzed with a 20 ms time bin.

For photobleaching measurements, the same CW laser (3 mW pump power) was used, but focused with a 1 inch lens, yielding a focused spot of ~200 μm^2 at the sample surface. A higher NQD density ensured dozens of NQDs were present within the focused laser area. Using a LN-cooled CCD camera, a series of PL emission images was recorded with a 1 s integration time (90 ms readout time) over 10,000 frames, resulting in a total measurement time of ~3 h.

X-ray diffraction (XRD) measurements were made on a Rigaku Ultima III diffractometer that uses a fine line sealed Cu tube Kα (λ= 1.5406Å) X-rays. The generator is a D/MAX Ultima series with a maximum power of 3 kW. The samples were mounted on a background-less silicon slide that was placed on top of a thin-film stage that was aligned for maximum sample height and X-ray intensity. Data were collected in continuous scan mode in parallel beam slit geometry over the 2-theta range from 10-90° with sampling width of 0.005° and a scanning speed of 0.100°/min. The source was held at various fixed angle ranging from 3° while the detector was allowed to collect over the 2-theta range from 10-90°. The divergence slit was set to 1.0 mm, the divergence H.L. Slit was set at 10 mm, and the scattering and receiving slits were set to open. Literature reports indicate that InP synthesized using this method form a zinc blende structure,[1] while our XRD results indicate that the CdS shell was of wurtzite lattice structure (Figure S1).

Theoretical model for InP/CdS core/shell heterostructure. For theoretical analysis we used an effective mass approximation and single band model for the conduction band electrons and valence band holes. The size range of the nanostructures corresponds to the strong confinement regime, in which the Coulomb interaction between the electrons and holes is weak compared to their kinetic energy and can be accounted for as a first order perturbation. Besides direct Coulomb interaction between the carriers, we also take into account the interactions between the carriers and their images produced by the core-shell interface and the surface polarization.

The detailed electronic structure calculations described in the literature[4] have been parameterized for InP/CdS materials. As described previously,[5] we adjusted the model to account for the electron effective mass dependence on the electron energy, ΔE_e, calculated from the bottom of the conduction band (and subsequently on the nanocrystal size) according to $m_e^*(\Delta E_e) = m_e/(\alpha + E_p/(E_g + \Delta E_e))$. In this expression we set $E_g = 1.34$ eV, $E_p = 20.6$ eV, and $\alpha = -1.2$, where m_e is the free electron mass. The InP hole effective mass is set to the bulk value $0.64m_e$. In CdS, the electron (hole) effective mass is set to the bulk parameter $0.21m_e$ ($0.68m_e$). The conduction (valance) band offset is calculated to be 0.39 eV (1.25 eV) below the bottom (top) of the band. This corresponds to the type-II heterostructure with an effective band gap of 0.95 eV (top of the core and bottom of the shell). The dielectric constants for the core, shell, and surrounding solvent are set to 9.6, 5.3, and 1.5, respectively.

Using the parameterization described above, we have computed the 1S exciton energy, which can approximately be identified as the PL energy. The calculation results for small core radii are shifted to the higher energies compared to experimental measurements. The discrepancy arises from the approximate nature of the adopted effective mass model. Specifically, in our calculations we do not account for the conduction-valence band coupling, variation of the hole effective mass with the InP core size, deviation from spherical symmetry, and the interface strain. Regardless this discrepancy, the accuracy of the adopted effective mass model allows us to clearly identify the type-II electron-hole localization regime.

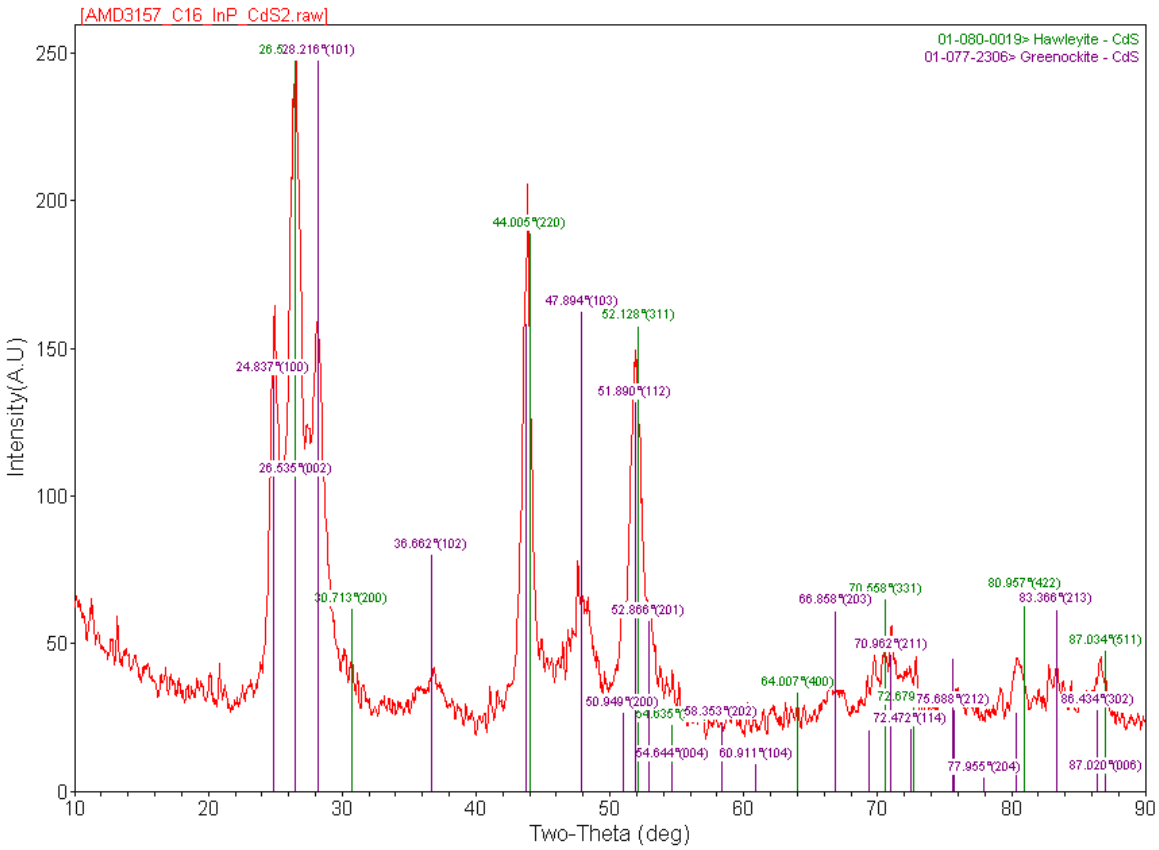

Figure S1: XRD of thick-shell InP/CdS. XRD analysis confirms that the CdS shell is characterized by a hexagonal (wurtzite) crystal structure.

Table S1: PL lifetime fit parameters.

	τ1 (ns)		τ2 (ns)		τ3 (ns)		average (ns)	Ref.
InP1	28.0	(67.0%)	73.0	(24.0%)	166.0	(9.0%)	83.6	6
InP2	16.1	(10.0%)	98.3	(75.0%)	262.0	(14.0%)	150.7	7
InP3	16.0	(21.0%)	77.9	(69.0%)	218.0	(10.0%)	114.0	7
InP4	11.9	(25.0%)	60.2	(67.0%)	191.0	(8.0%)	91.9	7
InP/ZnS1	17.0	(9.0%)	67.4	(73.0%)	219.0	(19.0%)	134.9	7
InP/ZnS2	20.0	(13.0%)	64.7	(69.0%)	245.0	(18.0%)	150.5	7
InP/ZnS3	23.9	(18.0%)	69.9	(65.0%)	265.0	(17.0%)	160.5	7
InP/1CdS	13.4	(41.6%)	64.1	(44.7%)	300.9	(13.7%)	189.9	
InP/2CdS	8.0	(43.5%)	81.6	(40.0%)	450.4	(16.4%)	326.9	
InP/3CdS	15.1	(33.8%)	106.8	(42.5%)	464.3	(23.8%)	349.2	
InP/4CdS	27.5	(29.0%)	147.9	(45.0%)	581.8	(26.1%)	434.6	
InP/7CdS	25.1	(16.0%)	167.7	(49.0%)	717.6	(35.0%)	575.4	
InP/10CdS	71.3	(35.2%)	326.6	(45.4%)	1052.4	(19.4%)	702.1	

REFERENCES:

1. Xie, R., Battaglia, D. & Peng, X. Colloidal InP nanocrystals as efficient emitters covering blue to near-infrared. *J. Am. Chem. Soc.* **129**, 15432-15433 (2007).
2. Xie, R.G., Li, Z. & Peng, X.G. Nucleation Kinetics vs Chemical Kinetics in the Initial Formation of Semiconductor Nanocrystals. *J. Am. Chem. Soc.* **131**, 15457-15466 (2009).
3. Jones, M. & Scholes, G.D. On the use of time-resolved photoluminescence as a probe of nanocrystal photoexcitation dynamics. *J. Mater. Chem.* **20**, 3533-3538 (2010).
4. Piryatinski, A., Ivanov, S.A., Tretiak, S. & Klimov, V.I. Effect of quantum and dielectric confinement on the exciton-exciton interaction energy in type II core/shell semiconductor nanocrystals. *Nano Lett.* **7**, 108-115 (2007).
5. Efros, A.L. & Rosen, M. The electronic structure of semiconductor nanocrystals. *Annu Rev. Mater. Sci.* **30**, 475-521 (2000).
6. Micic, O.I. et al. Size-dependent spectroscopy of InP quantum dots. *J. Phys. Chem. B* **101**, 4904-4912 (1997).
7. Li, C.L., Ando, M., Enomoto, H. & Murase, N. Highly Luminescent Water-Soluble InP/ZnS Nanocrystals Prepared via Reactive Phase Transfer and Photochemical Processing. *J. Phys. Chem. C* **112**, 20190-20199 (2008).